Single-Step Assembly of DOX/ICG Loaded Lipid–Polymer Nanoparticles for Highly Effective Chemo-photothermal Combination Therapy

Mingbin Zheng,[†,‡,§] Caixia Yue,[†,§] Yifan Ma,[†,§] Ping Gong,[†] Pengfei Zhao,[†] Cuifang Zheng,[†] Zonghai Sheng,[†] Pengfei Zhang,[†] Zhaohui Wang,[†] and Lintao Cai[†,*]

[†]Guangdong Key Laboratory of Nanomedicine, Shenzhen Key Laboratory of Cancer Nanotechnology, Institute of Biomedicine and Biotechnology, Shenzhen Institutes of Advanced Technology, Chinese Academy of Sciences, Shenzhen 518055, P.R. China and [‡]Department of Chemistry, Guangdong Medical College, Dongguan 523808, P.R. China. [§]Mingbin Zheng, Caixia Yue, and Yifan Ma equally contributed to this work.

ABSTRACT A combination of chemotherapy and photothermal therapy has emerged as a promising strategy for cancer therapy. To ensure the chemotherapeutic drug and photothermal agent could be simultaneously delivered to a tumor region to exert their synergistic effect, a safe and efficient delivery system is highly desirable. Herein, we fabricated doxorubicin (DOX) and indocyanine green (ICG) loaded poly(lactic-*co*-glycolic acid) (PLGA)–lecithin–polyethylene glycol (PEG) nanoparticles (DINPs) using a single-step sonication method. The DINPs exhibited good monodispersity, excellent fluorescence/size stability, and consistent spectra characteristics compared with free ICG or DOX. Moreover, the DINPs showed higher temperature response, faster DOX release under laser irradiation, and longer retention time in tumor. In the meantime, the fluorescence of DOX and ICG in DINPs was also visualized for the process of subcellular location *in vitro* and metabolic distribution *in vivo*. In comparison with chemo or photothermal treatment alone, the combined treatment of DINPs with laser irradiation synergistically induced the apoptosis and death of DOX-sensitive MCF-7 and DOX-resistant MCF-7/ADR cells, and suppressed MCF-7 and MCF-7/ADR tumor growth *in vivo*. Notably, no tumor recurrence was observed after only a single dose of DINPs with laser irradiation. Hence, the well-defined DINPs exhibited great potential in targeting cancer imaging and chemo-photothermal therapy.

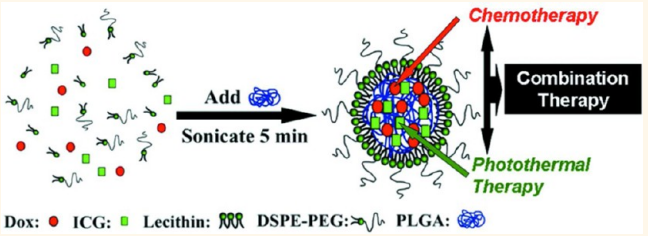

KEYWORDS: indocyanine green · doxorubicin · photothermal therapy · chemotherapy · multidrug resistance

Cancer therapy currently relying on a single therapeutic treatment remains unsatisfying. Combination therapy has been considered as a promising strategy to improve therapeutic efficiency and minimize side effects.[1,2] The combination of therapeutic approaches with different drugs and mechanisms may cooperatively suppress cancer development with potential advantages (*e.g.*, synergistic effects and reversal of drug resistance).[1−3] It had been reported that the delivery system loaded with a vascular shutdown combretastatin and an apoptosis-inducing doxorubicin (DOX) significantly suppressed the growth of melanoma and lung carcinoma as compared to either single-agent regimen.[4] The codelivery strategy that utilized siRNA to silence the expression of efflux transporter together with appropriate anticancer drugs had been used to overcome multiple drug resistance.[5] There also has been a great interest in developing combined treatment of near-infrared (NIR) thermotherapy and chemotherapy to augment the cytotoxicity of chemotherapeutic agents.[6,7] Thermotherapy based on photothermal agents that strongly absorb NIR light and convert it into cytotoxic heat for tumor treatment, such as indocyanine green (ICG), gold nanomaterials, or carbon nanotubes, has been demonstrated as a non-invasive, harmless, and highly efficient therapeutic technique.[8−10] Nevertheless, to exert their maximal cooperation effect, it is expected that the accurate doses of chemotherapeutic drug and photothermal agent should be simultaneously delivered to the same tumor cells after systemic administration.

* Address correspondence to lt.cai@siat.ac.cn.

Received for review September 17, 2012 and accepted February 15, 2013.

Published online February 15, 2013
10.1021/nn400334y

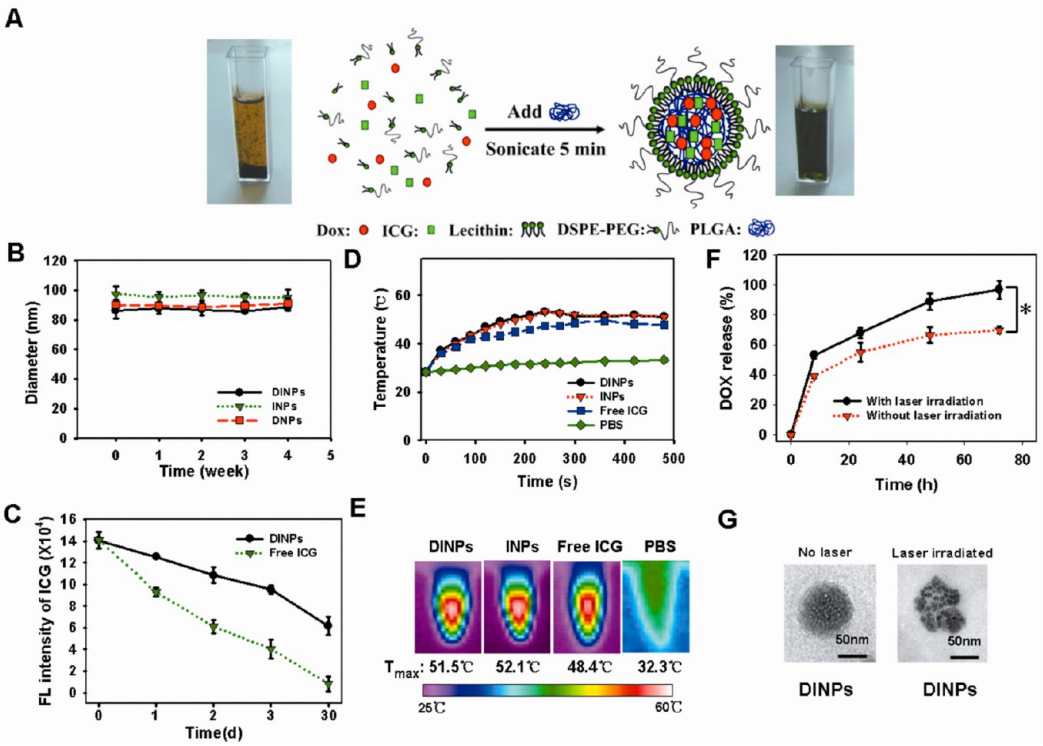

Figure 1. Synthesis and charecterization of DINPs. (A) Schematic illustration of the single-step sonication to synthesize DINPs. Photograph of mixture containing DOX, ICG, lecithin, and DSPE-PEG was before (left) and after (right) sonication. (B) Size stability test of DINPs, INPs, and DNPs. (C) ICG FL stability of DINPs and free ICG. (D) Maximum temperature profiles of DINPs, INPs, free ICG, and PBS as a function of the irradiation time under continuous laser irradiation at a power intensity of 1 W/cm^2. (E) Infrared thermographic maps of centrifuge tubes with DINPs, INPs, free ICG, or PBS were measured at 5 min with an infrared thermal imaging camera after continuous laser irradiation. (F) DOX release profiles from DINPs with and without laser irradiation. The data are shown as mean ± SD (n = 3); (*) P < 0.05, (**) P < 0.01. (G) TEM images of DINPs with or without continuous laser irradiation. After laser irradiation DINPs were broken up into smaller pieces with heat-induced disruption. It was consistent with the *in vitro* release experiments that the DOX release of DINPs could be accelerated by laser irradiation.

A variety of nanoparticle-based delivery systems capable of delivering dual or multiple drugs have been established[10,11] and can be divided into two major categories, that is, the lipid-based and polymer-based with liposomes and polymeric nanoparticles (NPs) as their typical representatives, respectively.[11−14] To date, a great deal of antitumor drugs based on liposomes and polymer NPs such as Doxil (DOX liposomes) and Genexol-PM (Taxol methoxy-polyethylene glycol (PEG) poly(D,L-lactide) NPs) have been approved by the Food and Drug Administration (FDA) for clinical use.[13] The lipid-polymer hybrid NPs can take the unique advantages of polymeric NPs and liposomes and become a robust drug delivery platform with high drug encapsulating, tunable, and sustained drug release, excellent serum stability, and potential for differential targeting of cells or tissues.[15−18] Docetaxel and yttrium^{90}-loaded lipid-polymer NPs have been developed and show much higher therapeutic efficacy than the respective chemotherapy or radiotherapy treatment.[16]

We recently reported ICG-loaded biodegradable folate-lipid-poly(lactic-*co*-glycolic acid) (PLGA) NPs for *in vitro*/*in vivo* tumor targeting imaging.[19] A PLGA NPs drug delivery system with simultaneous incorporation of chemotherapeutic (DOX) and thermo-optical agents (ICG) was developed.[20] On the basis of the encouraging results, the PLGA-lecithin-PEG NPs containing DOX and ICG (DINPs) were synthesized using a single-step sonication method. The ICG (DOX) could serve as a dual-functional agent with integrated photothermal therapy (chemotherapy) and optical imaging probes capabilities. The fluorescence (FL) of ICG or DOX in DINPs can be monitored to demonstrate subcellular localization and metabolic distribution. The cytotoxic effects of DINPs by combining therapeutic modalities of chemotherapy and hyperthermia in DOX-sensitive MCF-7 and DOX-resistant MCF-7/ADR cells were investigated. Moreover, the synergistic effect of combined treatment of DINPs was evaluated in comparison with chemo- or photothermal treatment alone, and also the suppression and remission for the MCF-7 and MCF-7/ADR xenograft tumors were investigated after a single dose treatment *in vivo*.

RESULTS AND DISCUSSION

Characterization of the DINPs. The synthesized process was described in Figure 1A. The DINPs were self-assembled from DOX, ICG, PLGA, lecithin, and DSPE-PEG through a single-step sonication method. In the mixture containing DOX, ICG, lecithin and DSPE-PEG,

green ICG would quickly aggregate and sedimentate. After PLGA added dropwise under sonication, the resulting mixture solution turned into clear dark green. Specifically, PLGA polymer coencapsulated DOX and ICG to form a core. Lecithin and DSPE-PEG self-assembled around the PLGA core to form a lipid monolayer covered by a PEG shell for the stabilization of the core.

The transmission electron microscopy (TEM) image of DINPs showed that the NPs were generally spherical in shape with good monodispersity (Supporting Information, Figure S1). The particle size, zeta potential, and size distribution were shown in Supporting Information, Table S1 and Figure S1. The zeta potential of DINPs, ICG loaded PLGA-lecithin-PEG NPs (INPs), and DOX loaded PLGA-lecithin-PEG NPs (DNPs) were between −21.71 and −26.22 mV. The hydrodynamic sizes of the DINPs, INPs, and DNPs were respectively 86.3, 97.6, and 90.1 nm with a polydispersity of 0.100−0.180; 99% DINPs in number distribution were all less than 100 nm, which will be suitable for passive tumor targeting of drug delivery through the enhanced permeability and retention effect (EPR).[21] The drug encapsulation efficiency (EE) and drug loading efficiency (LE) of the NPs are crucial for their clinical application. Supporting Information, Table S1 showed the EE or LE of the three types of NPs formulations. The EE or LE of DOX was observed at 43.75% or 6.91% for DNPs, and the EE or LE of ICG was 47.82% or 7.47% for INPs. The data demonstrated that DINPs encapsulated with the EE of 35.75% DOX and 32.73% ICG (loaded with the LE of 5.36% DOX and 4.91% ICG). Clearly, both the EE and LE of DINPs for DOX or ICG had slightly lower values compared with those of DNPs or INPs.

The absorption or FL spectra of encapsulated DOX and ICG were shown in Supporting Information, Figure S2. Compared with free ICG, the absorption or emission peak of DINPs was only red-shifted 1 nm to 778 nm or 6 nm to 815 nm. Absorption and emission peak corresponding DOX in DINPs was located at 480 and 591 nm, consistent with the spectra of free DOX. These data indicated that both the ICG and DOX maintained their optical properties after encapsulation with lipid-PLGA NPs. The particle sizes of DINPs, INPs, and DNPs remained around the initial particle size without aggregation and precipitation over one month (Figure 1B), suggesting a great stability of DINPs, DNPs, and INPs.

ICG is a FDA-approved dual-functional agent and has been applied in optically mediated diagnostic and photothermal therapy. However, application of ICG is limited by its numerous disadvantageous properties in aqueous solution, including its concentration-dependent aggregation and poor aqueous stability *in vitro*.[19,22] Additionally, ICG is highly bound to nonspecific plasma proteins, leading to rapid elimination from the body.[19,22] A number of nanometer-sized encapsulation systems, including PLGA NPs, phospholipid emulsions, and copolymer micelles, have been developed to protect ICG from degradation.[19,22,23] FL measurement illustrated that, after 1 day, FL intensity of ICG in DINPs remained nearly 90%, while FL intensity of free ICG decreased to 65.73% of initially intensity. Moreover, the FL intensity of free ICG was degraded to 5.80% within 30 days, while the FL intensity of ICG in DINPs remained above 44% (Figure 1C). These data suggested that the FL stability of ICG was significantly improved by encapsulation of NPs. The protective effect of NPs seemed to be due to the polymeric-envelope which protected the entrapped ICG by isolating it from the surrounding environment.[24]

To evaluate the photothermal efficiency of DINPs, we monitored the temperature changes under laser irradiation *in vitro* using an infrared thermal imaging camera. With the laser irradiation at 1 W/cm^2 for 8 min, the temperature of DINPs, INPs, and free ICG maximally increased to 53.2, 53.1, and 49.5 °C, while the PBS only increased by 5.1 °C (Figure 1D). Such a variation of DINPs, INPs, or free ICG could increase temperature over 43 °C, leading to an irreversible damage to tumor cells.[24,25] DINPs and INPs formulation had a higher temperature response than free ICG under laser irradiation, similar to that of previously reported ICG-containing lipid NPs which was more efficient in producing a laser-dependent temperature increase than ICG alone.[26] The possible reasons were that ICG encapsulated in DINPs or INPs had higher condensed concentration than free ICG, and the excitation thermal radiation was also entrapped in the enclosure of NPs, resulting in the higher energy efficiency and lower heat dissipation in the DINPs or INPs after laser irradiation. The infrared thermographics showed that the maximum temperature (T_{max}) of DINPs, INPs, free ICG, and PBS at 5 min after laser irradiation reached 51.5, 52.1, 48.4, and 32.3 °C (Figure 1E). Furthermore, laser irradiation accelerated DOX releasing from the DINPs, as shown in Figure 1F; the NPs without laser irradiation showed DOX release of 39.13% by 8 h and the total release reaching 69.86% by 72 h. The laser irradiation significantly increased the release rate of DOX from DINPs to 53.20% over the first 8 h. After laser irradiation, the total release of DOX by 72 h was significantly enhanced to 97.00%, indicating that the drug release of DINPs could be controllable by laser irradiation. We further studied the morphology of DINPs irradiated by 1 W/cm^2 808 nm laser for 5 min using TEM. Figure 1G showed that DINPs were broken up into smaller pieces with heat-induced disruption. It was consistent with the *in vitro* release experiments that the DOX release of DINPs could be accelerated by laser irradiation.

***In Vitro* Cellular Uptake.** The subcellular localization of free DOX, free ICG, and DINPs in MCF-7 and MCF-7/ADR cells was investigated using confocal microscopy. After 4 h incubation, free DOX mainly localized in the

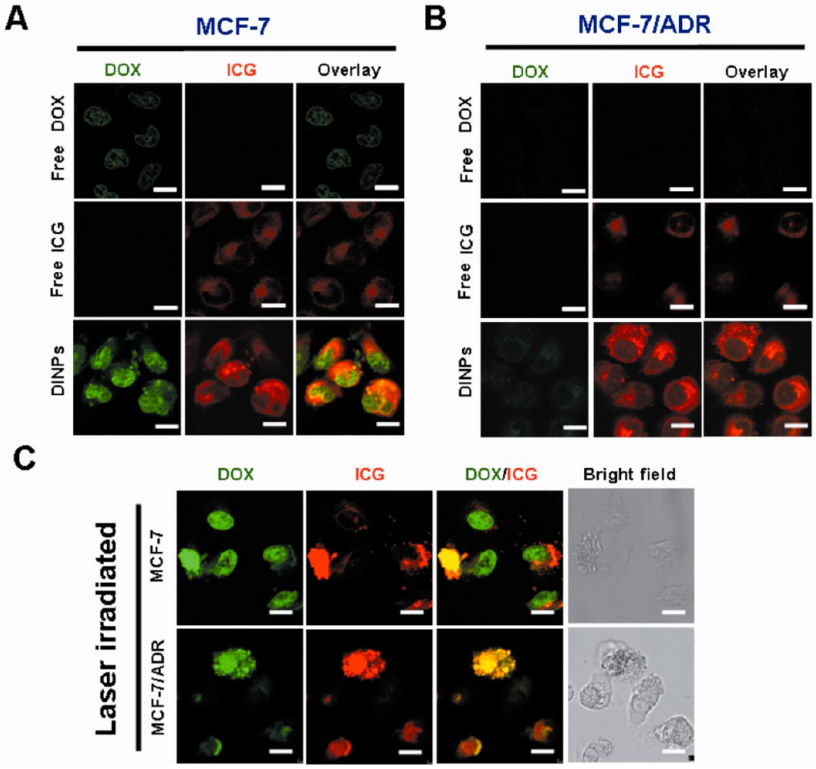

Figure 2. Endocytosis of DINPs by MCF-7 and MCF-7/ADR cells. (A) MCF-7 subcellular localization of free DOX, free ICG, and DINPs after 4 h incubation. Green represented FL of DOX, red represented FL of ICG. (B) MCF-7/ADR subcellular localization of free DOX, free ICG, and DINPs after 4 h incubation. (C) MCF-7 and MCF-7/ADR subcellular localization of DINPs after laser irradiation and 4 h incubation (scale bar, 15 μm).

cell nucleus in MCF-7 cells, consistent with a previous report[27] (Figure 2A). In contrast, only a very little amount of DOX was observed in the nucleus of MCF-7/ADR cells (Figure 2B). The decreased nuclear localization of DOX in MCF-7/ADR cells could be due to the presence of the P-glycoprotein efflux pump, which decreased drug accumulation in the cells.[27] On the other hand, ICG was homogenously distributed in the cytoplasm in both MCF-7 and MCF-7/ADR cells, which was consistent with a previous report that ICG mainly bonded to intracellular protein (glutathione S-transferase) (Figure 2A,B).[27] DINPs without laser radiation significantly increased the FL signals of DOX and ICG in both MCF-7 and MCF-7/ADR cells, indicating enhanced internalization of drugs by NP formulation (Figure 2A,B). Interestingly, DINPs-encapsulated DOX could be detected both in the cytosol and the nucleus of MCF-7 cells (Figure 2A). The possible reason could be that DOX molecules released from the NPs entered into the cell nucleus, while DOX entrapped in NPs was still in the cytosol because of size limitation, which prevented the NPs from traversing the nuclear pore complex. Although DINPs increased the uptake of DOX and ICG in MCF-7/ADR cells, DOX was mainly localized in the cytosol rather than in the nuclear and the amount of intracellular DOX was much less than that in MCF-7 cells (Figure 2A,B). Hence, DINPs formulation without laser radiation failed to overcome the P-glycoprotein efflux pump mechanisms.

Notably, DINPs formulation with laser radiation not only significantly increased the FL signals of DOX and ICG in MCF-7 and MCF-7/ADR cells, but also facilitated them entry into the nuclei (Figure 2C). These phenomena could be due to the laser-caused hyperthermia, which increased cell permeability and fluidity, thereby enhancing the drug accumulation inside cancer cells.[27] Moreover, the hyperthermia also severely resulted in damaged cells including loss of nucleus, cell shrinkages, or coagulation.[8] Also, the heat caused by laser radiation could disrupt DINPs into smaller pieces, which would be easier to enter into the cells and nuclei. Taking these factors into consideration, it is not surprising that hyperthermia significantly increased the uptake of ICG and DOX in MCF-7 and MCF-7/ADR cells.

***In Vitro* Chemothermal, Photothermal, and Chemo-photothermal Treatments.** MCF-7 cells and MCF-7/ADR cells demonstrated different sensitivity to DINPs without laser radiation (Figure 3A,B). After 24 h incubation, DINPs containing 6 μg/mL DOX killed 87.70 or 13.23% of cells in MCF-7 or MCF-7/ADR cells, respectively. These results were in accordance with previous observation that DINPs enhanced the uptake of DOX more effectively in MCF-7 cells than in MCF-7/ADR cells.[27] The MCF-7/ADR cells were more resistant to DOX compared with

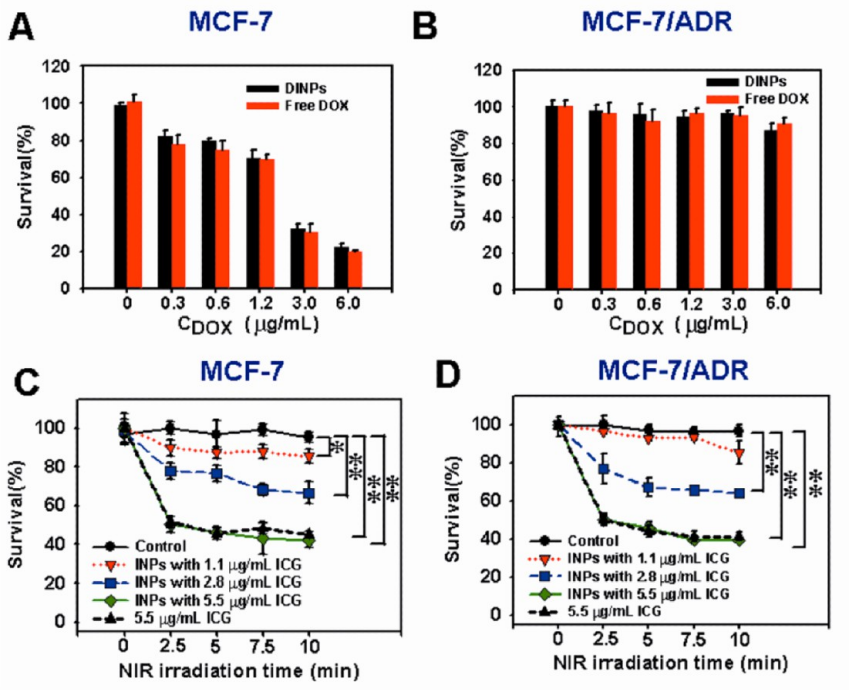

Figure 3. The chemothermal and photothermal treatments in MCF-7 and MCF-7/ADR cells. (A) Quantitative evaluation of cell survival for MCF-7 cells treated with free DOX and DINPs for 24 h. (B) Quantitative evaluation of cell survival for MCF-7/ADR cells treated with free DOX and DINPs for 24 h. (C) Survival of MCF-7 cells *versus* ICG concentration in INPs and laser irradiation time. (D) Survival of MCF-7/ADR cells *versus* ICG concentration in INPs/free ICG and laser irradiation time.

the drug-sensitive MCF-7 cells, and DINPs encapsulation did not affect the anticancer effect of DOX in the MCF-7 and MCF-7/ADR cells (Figure 3A,B). Intracellular DOX concentration of DINPs could be enhanced by DINPs-mediated cellular uptake, but reduced by the sustained release of DOX. All of these eventually led to similar DOX concentration in cells and very close cytotoxicity of DINPs, compared with free DOX. No cytotoxicity was observed in the MCF-7 and MCF-7/ADR cells treated with 200 μg/mL empty NPs locating at the zero position of DINPs, indicating that empty NPs were biocompatible at this concentration (Figure 3 A,B).

We further quantitatively investigated the effect of irradiation time and ICG concentration in INPs on cell death at 1.6 W/cm^2 (Figure 3C,D). Without irradiation, treatment of INPs containing different amount of ICG did not affect growth of MCF-7 or MCF-7/ADR cells, suggesting their great biocompatibility (Figure 3C,D). The results also showed that the MCF-7 cells treated with INPs containing 1.1 μg/mL ICG were killed 12.45 and 14.56% under 5 and 10 min laser irradiation, respectively (Figure 3C). While treated with INPs containing 5.5 μg/mL ICG, the death rate of MCF-7 cells was significantly increased to 53.54 and 58.12% after 5 and 10 min laser irradiation (Figure 3C). Concentrations of 5.5 μg/mL ICG were not significantly different from the INPs containing the same concentration of ICG, possibly stemming from the little temperature differences of free ICG and INPs after irradiation (Figure 3C). The viability of MCF-7/ADR cells *versus* ICG concentration in INPs and laser irradiation time was very similar to those of MCF-7 cells, indicating MCF-7/ADR cells had similar sensitivity to heat (Figure 3C,D).

To visually evaluating the efficiency of the DINPs, the MCF-7 cells in the presence of DINPs were treated with or without laser irradiation of 1.6 W/cm^2. The cells were stained with calcein-AM and PI to identify live and dead/late apoptotic cells, respectively. Figure 4A and Supporting Information, Figure S3 showed that laser irradiation alone without DINPs did not affect cell viability, suggesting laser irradiation at the power density of 1.6 W/cm^2 was safe for MCF-7 cells. Incubation with DINPs for 24 h caused about 80% of cell death as demonstrated by significantly reduced cell density. Moreover, the combination of DINPs with laser irradiation further induced cell death up to 96.90%, suggesting the amount of ICG was sufficient for photothermal therapy. The cytotoxic effect of chemo-photothermal treatment on MCF-7 cells was further quantified by flow cytometry (Figure 4B). MCF-7 cells were treated with DINPs for 6 h with or without laser irradiation, and then labeled with PI and Annexin V. The PI$^+$ Annexin V$^+$ cells were defined as late apoptotic/necrotic cells. The results showed that DINPs plus laser more significantly induced cell late apoptosis/necrosis (86.9%) as compared with those treated by laser (0.7%) or DINPs (15.3%). The results suggested that the cytotoxic effect of DINPs on MCF-7 cells could be boosted by the laser irradiation.

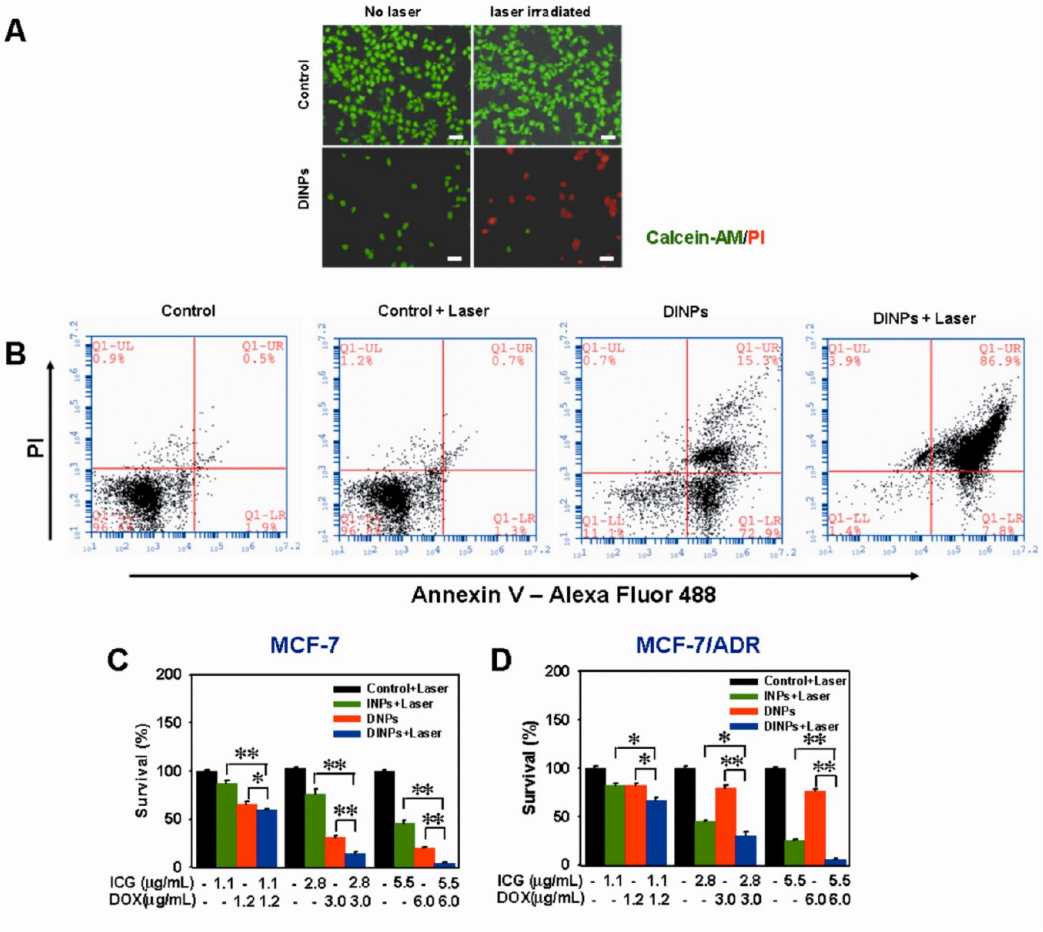

Figure 4. Cell survivals of MCF-7 or MCF-7/ADR cells after chemo-photothermal treatment. (A) FL images of MCF-7 cells after chemo-photothermal treatment. Viable cells were stained green with calcein-AM, and dead/later apoptosis cells were floating and eluted, or stained red with PI. (scale bar, 35 μm). (B) Flow cytometry analysis of MCF-7 cells after chemo-photothermal treatment. (C) Quantitative comparison of MCF-7 cells viability following chemo (DNPs), photothermal (INPs + laser), and chemo-photothermal treatments (DINPs + laser) for 24 h. (D) Quantitative comparison of MCF-7/ADR cells viability following chemo (DNPs), photothermal (INPs + laser) and chemo-photothermal treatments (DINPs + laser) for 72 h. The data are shown as mean ± SD (n = 3); (*) P < 0.05, (**) P < 0.01.

As expected from the quantitative results, the chemo-photothermal treatments resulted in significantly lower viabilities than chemo or photothermal treatment alone (Figure 4C,D). The survival at 24 h of MCF-7 cells treated with INPs containing 5.5 mg/mL ICG plus laser irradiation was 13.88%, and the survival of cells treated with DNPs containing 6.0 mg/mL DOX was 59.65%. However, when the cells were treated with DINPs containing ICG and DOX with the same concentrations plus laser irradiation, the survival of cells was significantly reduced to 4.09%. With the treatments of INPs (5.5 mg/mL of ICG), DNPs (6.0 mg/mL of DOX), and DINPs (5.5 mg/mL of ICG and 6.0 mg/mL of DOX) plus laser radiation, the survival of MCF/ADR cells at 72 h was 30.53%, 66.43%, and 5.26%, respectively. The combination of DINPs and laser irradiation was more effective than either treatment alone to induce cell death in both MCF-7 and MCF-7/ADR cell cultures.

***In Vivo* Imaging and Biodistribution.** To deliver drugs into tumor tissues, the NPs-based drug must enter into the tumor vasculature and interstitium. The NPs could be retained there and diffuse drug into the cells.[28,29] Xenograft tumors in nude mice have been reported to be more invasive than *in situ* carcinoma and can form the construction of a capillary network.[30] It would allow the enrichment of nanomedicines in tumors due to the EPR effect. One of the important concerns after intratumoral injection is whether the DINPs would accumulate in xenograft tumor or organs or clear out of the body. By utilizing the intrinsic and sensitive laser FL of ICG, the amounts of DINPs accumulated in tumor and organs were measured without additional radio- or fluorescent labeling. Figure 5A,B showed the ICG FL signal and intensity distribution around the tumor after intratumoral injections of free ICG and DINPs. The FL signals in whole bodies of mice, except for the peritumor, were relatively weak because of a relatively low dose of ICG in other areas. The ICG FL intensity around the tumor at 6, 12, and 24 h postinjection for DINPs reduced to 87.10%, 59.84%, and 42.97% of initial FL

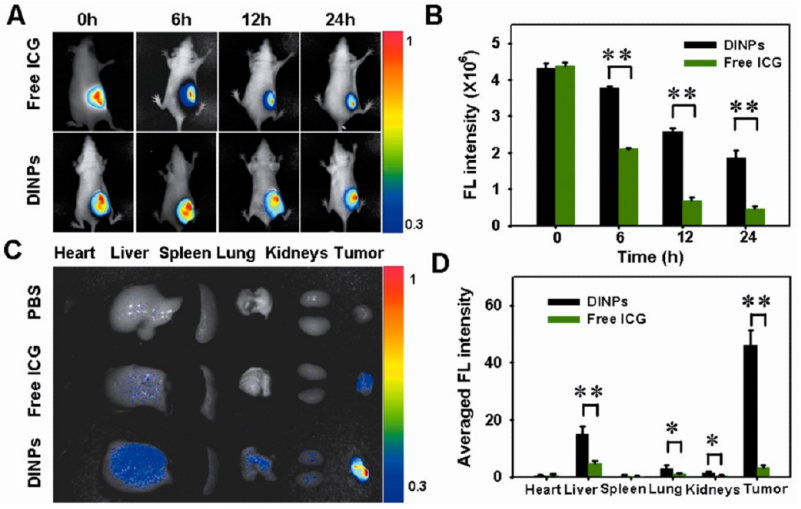

Figure 5. ***In vivo*** **imaging and biodistribution of nude mice bearing MCF-7 tumors after intratumoral injection of free ICG or DINPs. (A)Time-lapse NIR FL images of nude mice. (B) NIR FL intensities around the tumor were quantified at indicated time points. (C) NIR FL images of major organs and tumors after injection of PBS, free ICG, and DINPs at 24 h. (D) Semiquantitative biodistribution of free ICG and DINPs in nude mice determined by the averaged FL intensity of organs and tumor. The data are shown as mean ± SD (n = 3); (∗) P < 0.05, (∗∗) P < 0.01.**

intensity. For free ICG, the corresponding results were 47.73%, 15.49%, and 10.70%. In contrast, the DINPs were significantly retained around the tumor even after 24 h. These results could be attributable to the prolonged retention time of ICG in the tumor caused by the tumor passive targeting of EPR effects, and reduced ICG degradation by DINPs encapsulation. The relatively faster FL decrease of free ICG is also attributed to FL quenching of free ICG in physiological environments with rapid aggregation and clearance from the body.[31]

The comparative major organs and tumors distribution of free ICG and DINPs were shown in Figure 6C,D. The results demonstrated that most of ICG accumulated in the liver and tumor 24 h after intratumoral injection of free ICG. DINPs formulation dramatically increased the accumulation of ICG in the tumor, followed by liver, lung, and kidneys. The averaged FL intensity in tumor was more than 13 times than that of free ICG formulation. Considering the liver-specific distribution of ICG itself and reticuloendothelial system (RES) uptake of particulates in circulation, these data were in accordance with the reported pharmacokinetics assay.[32]

In Vivo **Chemothermal, Photothermal and Chemo-photothermal Treatments.** We measured the intratumoral temperature while the tumor region intratumoral injected with PBS, free ICG, and DINPs was irradiated by 1 W/cm^2 NIR laser for 8 min (Figure 6A). After the 8 min of laser irradiation, the tumors treated with free ICG, INPs, and DINPs had a maximum temperature of 52.8, 57.0, and 56.9 °C, which exceeds the damage threshold needed to induce irreversible tissue damage.[33] The maximum temperature of DINPs, INPs, free ICG at 5 min after laser irradiation

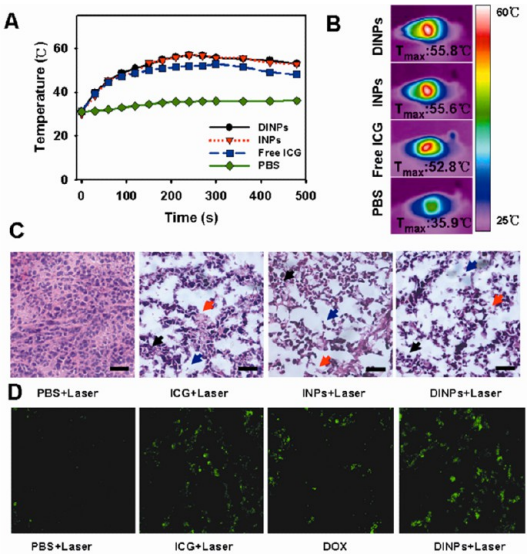

Figure 6. Temperature increase in MCF-7 tumor tissues and histologic assessments after photothermal therapy or chemotherapy. (A) Maximum temperature profiles of the irradiated area of nude mice bearing tumors injected with DINPs, INPs, free ICG, or PBS as a function of the irradiation time. (B) Infrared thermographic maps of mice intratumoral injected with DINPs, INPs, free ICG, or PBS were measured at 5 min after laser irradiation. (C) Histological staining of the excised tumors at 12 h after injection of PBS, free ICG, INPs, and DINPs under laser irradiation. Common features of thermal damage were identified in tumors treated with free ICG, INPs, and DINPs, such as coagulative necrosis (black arrow), abundant pykonosis (blue arrow), and considerable regions of karyolysis (red arrow). (Scale bar, 50 μm). (D) Cellular apoptosis of MCF-7 cells in tumor tissues induced by PBS plus laser, free ICG plus laser, free DOX and DINPs plus laser. The apoptotic cells labeled green FL were evidently identified by TUNEL assay. The tumor cells treated with ICG plus laser or DOX exhibited a great number of apoptosis signals because both hyperthermia and DOX could cause cell apoptosis. The degree of apoptosis was significantly higher in the DINPs plus laser group.

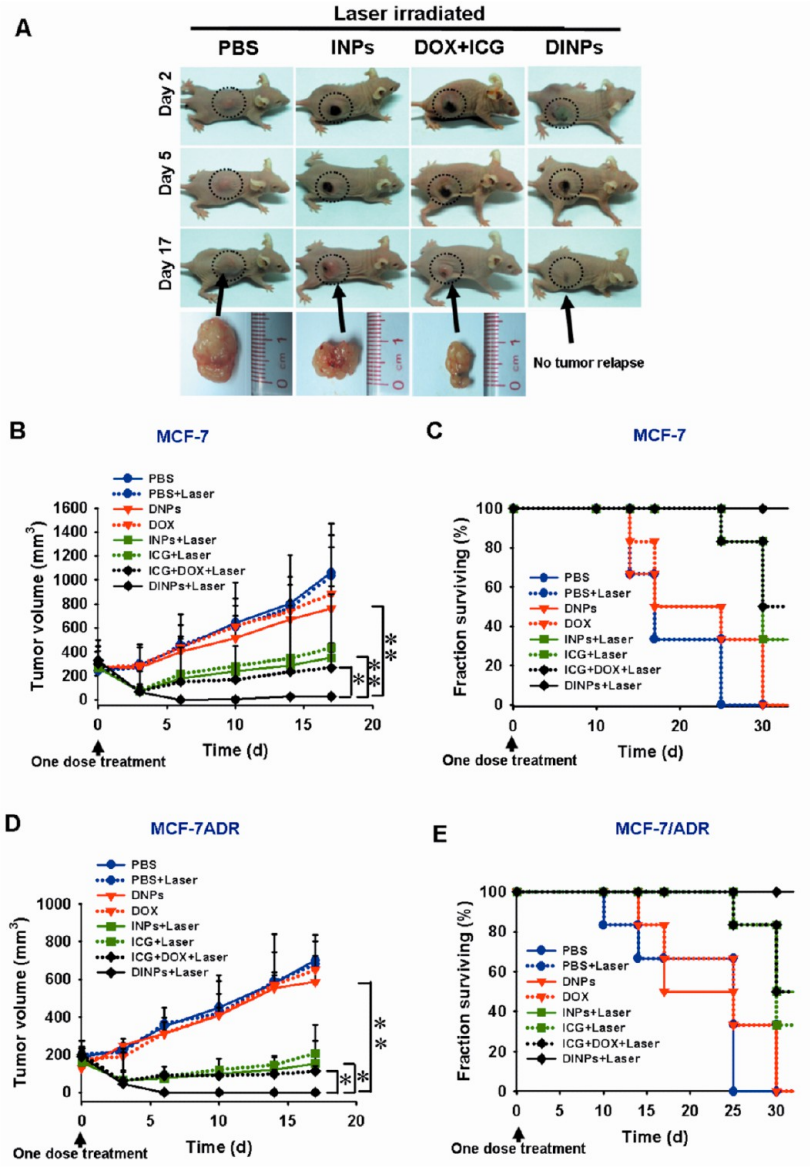

Figure 7. ***In vivo*** **chemo-photothermal therapy of DINPs. (A) Representative photos of mice bearing MCF-7 tumors and excised tumors on 17 d after treatments. The tumors were marked with dashed circles. Combined treatment of DINPs yielded higher synergistic therapy effect and no tumor recurrence was noted over a course of 17 days. (B) MCF-7 tumor growth curves of different groups after treatments. (C) Survival rates of mice bearing MCF-7 tumors after treatments. (D) MCF-7/ADR tumor growth curves of different groups after treatments. (E) Survival rates of mice bearing MCF-7/ADR tumors after treatments; (*)** $P < 0.05$**, (**) **$P < 0.01$.**

reached 55.8, 55.6, 52.8 °C at the irradiated area; however, the PBS-treated tumor for the same laser irradiation resulted in a temperature increase of 5.2 °C (Figure 6B), that is insufficient to irreversibly damage the tumor.[32,34]

To further determine the antitumor effect of DINPs mediated chemo-photothermal therapy *in vivo*, MCF-7 tumor tissues were stained with hematoxylin and eosin or were detected by the TUNEL assay. As shown in Figure 6C, the tumors treated with free ICG, INPs, and DINPs plus laser irradiation demonstrated typical features of thermal damage, such as coagulative necrosis, abundant pykonosis, and considerable regions of karyolysis in tumors as described previously.[26,29] According to the results of TUNEL assay in which apoptosis cells were labeled green FL (Figure 6D), both ICG plus laser and DOX led to a significant number of apoptotic cells, and the combination of DINPs plus laser group further promoted apoptosis in MCF-7 tumor tissues.

We first investigated the anticancer effect of chemo-photothermal therapy in nude mice bearing MCF-7 tumors. The results showed that the tumors treated with PBS or PBS plus laser irradiation grew rapidly, suggesting the MCF-7 tumor growth was not affected by laser irradiation (Figure 7A,B). The growth of MCF-7 tumors was slightly inhibited by DNPs or by free DOX without significant difference (Figure 7B). Although

DOX is a well-known chemotherapeutic agent to a MCF-7 tumor, it usually requires multiple and high dosages to achieve a satisfying anticancer effect. In the present study, mice were treated with only a single dose of DOX, which was certainly not sufficient to suppress tumor growth *in vivo*. For mice treated with INPs or ICG plus laser irradiation, although no tumor recurrence was seen in the tumor site with black scar, tumor surrounding the scar grew rapidly afterward, and the survival rate of these two groups was 33.3% on day 30 post-treatment (Figure 7A–C). Surprisingly, a single injection of DINPs plus laser irradiation led to a complete remission of MCF-7 tumors, leaving the original tumor site with black scars which fell off about 2 weeks later (Figure 7A,B). No tumor recurrence was observed in this group over a course of 30 days (Figure 7A–C). Notably, the treatment of free ICG/DOX plus laser irradiation inhibited tumor growth less effectively than DINPs plus laser with 50% of the survival rate on day 30, which could be attributable to the shorter retention time of DOX and lower temperature increase (Figure 7A–C).

The anticancer effect of the chemo-photothermal treatment was also investigated in the mice bearing MCF-7/ADR tumors. The administration of free DOX or DNPs did not significantly inhibit the growth of MCF-7/ADR tumors (Figure 7D). The combination of laser irradiation with ICG, INPs, or ICG/DOX significantly suppressed the tumor growth, of which the survival rate was 33.33%, 50%, and 50% on day 30 (Figure 7D,E). The combination of DINPs with laser irradiation led to complete remission of tumors with 100% of survival rate on day 30, confirming their synergistic effect on tumor regression and the capability of overcoming multidrug resistance (Figure 7D,E). The potent anticancer effect of DINPs with laser irradiation could be attributable to efficient cooperation of ICG-mediated thermal toxicity and DOX-mediated cytotoxicity as well as extended retention time of NPs in tumors. Overall, the combination treatment of DINPs with laser irradiation demonstrated remarkable anticancer efficacy in both DOX-sensitive and DOX–resistant breast cancers, and gave a satisfying survival rate with significant elongation of life span for mice.

By seeing the synergistic anticancer effect of NPs-based chemotherapy and photothermal therapy, it would be interesting to determine whether photothermal therapy could enhance the anticancer effect of commercialized Caelyx (pegylated liposomal doxorubicin hydrochloride). The results showed that Caelyx alone failed to inhibit MCF-7/ADR tumor growth *in vivo*, which is possibly due to its insensitivity to DOX and a single injection of the drug (Supporting Information, Figure S4A). On the other hand, the coinjection of Caelyx and ICG combined with laser irradiation significantly inhibited tumor growth with the survival rate at 50% on day 30, which was similar to that of the ICG/DOX plus laser group (Supporting Information, Figure S4A,B). These data further confirmed the NPs-mediated chemo-photothermal therapy as a promising therapeutic strategy for cancer therapy.

The potential adverse effect of anticancer therapy remains a big concern for future clinical applications. In the present study, the loss of body weight was analyzed as an indicator for treatments-induced toxicity (Supporting Information, Figure S5A,B). On day 17, the control groups treated with PBS or PBS plus laser in nude mice bearing MCF-7 or MCF-7/ADR increased their body weights by 6–11%, and those treated with the ICG, INPs, or DINPs plus laser in nude mice bearing MCF-7 or MCF-7/ADR increased by 6–12%. These groups were not significantly different from the control group, which suggested that these treatments were well tolerated. Mice treated with DOX, ICG/DOX plus laser, DNPs, Caelyx, or Caelyx/ICG plus laser had body weights growth of 2–8% at day 17 in nude mice bearing MCF-7 or MCF-7/ADR. The weight growths were not significantly different from the control groups, indicating that DOX concentration of these groups injected with a single dose was well tolerant in nude mice bearing MCF-7 or MCF-7/ADR. Cardiac injury is a major complication of the oxidative stress-generating DOX.[35] We further investigated the potential cardiotoxicity of DOX or DINPs in MCF-7 tumor bearing mice. Mice were treated with free DOX, ICG plus laser, and DINPs plus laser. On day 17, hearts were removed and subjected to H&E staining. We did not observe any abnormality in heart tissues, suggesting no significant cardiotoxicity of current treatments, which can be due to only one dosage rather than multiple dosages (Supporting Information, Figure S6). These data suggested that the combined chemo-photothermal therapy with a single-dose treatment did not cause significant adverse effect *in vivo*.

CONCLUSIONS

We successfully fabricated the well-defined DINPs using a single-step sonication method, which could simultaneously deliver DOX and ICG to tumor regions for combined chemo-photothermal therapy. The DINPs remarkably enhanced ICG stability, produced higher localized temperature than free ICG after laser irradiation, and effectively promoted cellular uptake of DOX and ICG. The combination of chemo-photothermal therapies not only synergistically induced DOX-sensitive MCF-7 or DOX-resistant MCF-7/ADR cell death *in vitro*, but also suppressed MCF-7 or MCF-7/ADR tumor growth

and prevented tumor recurrence *in vivo*. Hence, the combination treatment of DINPs plus laser could be a promising strategy for chemo-photothermal cancer therapy.

MATERIALS AND METHODS

Materials. ICG, PLGA (MW, 5000−15000; lactide, glycoli-de (50:50)), 3-(4,5-dimethylthiazol-2-yl)-2,5-diphenyltetrazolium bromide (MTT), hematoxylin and eosin were purchased from Sigma-Aldrich (USA). Doxorubicin was purchased from Jinhe (China). Soybean lecithin, (1,2-distearoyl-*sn*-glycero-3-phosphoethanolamine-*N*-maleimide (polyethylene glycol 2000) (DSPE-PEG) were obtained from Avanti (USA). Calcein-AM and Alexa Fluor 488 Annexin V/Propidium Iodide (PI) Cell Apoptosis Kit were obtained from Invitrogen (USA). Caelyx pegylated liposomal doxorubicin hydrochloride was purchased from Schering-Plough (USA). Fetal bovine serum, RMPI 1640, DMEM, trypsin-EDTA and penicillin-streptomycin were purchased from Gibco Life Technologies (USA). One Step TUNEL apoptosis Assay Kit was obtained from KeyGEN (China). Amicon ultra-4 centrifugal filter with a molecular weight cutoff of 10 kDa was bought from Millipore (USA).

Formulation of DINPs. DINPs were synthesized from PLGA, soybean lecithin, DOX, ICG, and DSPE-PEG using a previously reported single-step sonication method.[36] PLGA was dissolved in 80% acetonitrile aqueous solution at a concentration of 2 mg/mL. To generate DINPs, (lecithin)/(DSPE-PEG) (mass ratio was 2:3) with a total mass ratio of 15% to the PLGA polymer, 750 μg DOX, and 750 μg ICG were added in 3 mL of 4% ethanol aqueous solution, and PLGA solution was added dropwise under sonication using an ultrasonics processor (VCX130, USA) at a frequency of 20k Hz and power of 130 W for 5 min. Finally the DINPs were washed three times using an Amicon ultra-4 centrifugal filter. The same procedures were used to prepare the INPs or DNPs in the absence of DOX or ICG.

Characterization of the DINPs. Size, surface charge, polydispersity, and size distribution of the NPs were obtained using Beckman Coulter DelsaTM Nano C (Beckman, USA) at room temperature. The morphologic and particle size examination of NPs were further performed by TEM (JEM-100XII) with negative stain method. Before analysis, the samples were stained with 2% (w/v) phosphotungstic acid, and then placed on copper grid with films and air-dried prior to imaging.

The EE and LE of DOX or ICG loaded in NPs was determined as follows: before ultrafiltration, the fresh NPs were isolated from the aqueous suspension medium by Beckman OptimaTM MAX-XP Ultracentrifuge (25 000 r/min, 30 min) (Beckman, USA). The nonentrapped DOX and ICG in the supernatant was determined by fluorescence spectroscopy (F900, Edinburgh Instruments Ltd., UK) with emission at 593 nm and excitation at 480 nm to monitor DOX, and emission at 815 nm and excitation at 740 nm to monitor ICG. The EE and LE are expressed according to the following formula: EE (%) = ((weight of loaded drug)/(weight of initially added drug)) $\times$ 100; LE (%) = ((weight of loaded drug)/(total weight of NPs)) $\times$ 100.

In vitro drug release profile of DINPs were determined by loading 1 mL of DINPs samples into dialysis tubing (MW, 12 000), which was submerged into 2 L of phosphate-buffered saline (PBS, pH = 7.4) as dissolution media. The release experiments were performed with and without 1 W/cm^2 808 nm laser irradiation (5W, Leimai, China) for 5 min at initial time of experiment at 37 °C. The morphologic changes of NPs with and without laser irradiation were also performed by TEM. The mixture was then incubated in a water bath at 37 °C under continuous shaking. At predetermined time points, the dialysate was taken out to estimate the amount of drug released, while the same amount of fresh PBS was added back and kept in a shaker for further study. The DOX concentration in the samples was measured by fluorescence spectroscopy, as described above.

The absorption spectra of free DOX, ICG, and DINPs were obtained using Perkin-Elmer Lambda25 UV/vis spectrometer (USA). Fluorescence spectra were obtained using fluorescence spectroscopy with excitation at 480 nm to monitor DOX and at 740 nm to monitor ICG. Fluorescent intensity at 815 nm of ICG and DINPs at different times was measured to identify ICG concentration at different times in ultrapure water. The ICG concentration was adjusted to 0.01 mg/mL.

Tumor Cells. DOX-sensitive (MCF-7) and DOX-resistant (MCF-7/ADR) human breast adenocarcinoma cells were used for the cell studies. Cells were grown in RMPI 1640 (for MCF-7) and DMEM (for MCF-7/ADR) culture medium containing 10% fetal bovine serum and 1% penicillin and 1% streptomycin at 37 °C under 5% CO_2. The MCF-7/ADR cells were maintained continuously in 0.5 μM of DOX.

***In Vitro* Cellular Uptake.** MCF-7 or MCF-7/ADR cells (2 $\times$ 10^4 cells/well) were seeded into 8-well chambered coverglasses (Lab-Tek, Nunc, USA) in 200 μL of medium, respectively. After 24 h, the medium was replaced by the medium containing DOX (18.00 μg/mL), ICG (16.48 μg/mL), or DINPs (18.00 μg/mL DOX and 16.48 μg/mL of ICG). After 4 h incubation, the cells were washed thrice with PBS and fixed with 4% paraformaldehyde solution for 20 min, then washed thrice with PBS, finally the fixed cells were observed by confocal laser scanning microscope (Leica TCS SP5, GER). The FL was imaged at λ_{EX} (488 nm) for DOX and at λ_{EX} (633 nm) for ICG. The MCF-7 or MCF-7/ADR cells incubated with DINPs (18.00 μg/mL DOX and 16.48 μg/mL of ICG) for 2 h were exposed to 1.6 W/cm^2 808 nm laser irradiation for 5 min, and the cells were incubated for another 2 h and further investigated the photothermal influence on cellular uptake.

***In Vitro* Chemothermal Photothermal, and Chemo-photothermal Treatments.** The MCF-7 cells were seeded into 96-well plate (1 $\times$ 10^4 cells/well) in 100 μL of medium. To directly observe the chemo-photothermal therapeutic efficacy, the medium was replaced by the medium with DINPs containing 6.0 μg/mL DOX and 5.5 μg/mL of ICG, and the medium without NPs as control. After 24 h incubation, the plate was placed on the Labnet AccublockTM digital dry bath incubator so that the wells remained at 37 °C prior to the application of the laser. The cells were irradiated with a 1.6 W/cm^2 808 nm laser for 5 min for chemo-photothermal treatments, whereas for chemotherapy alone, the cells were not exposed to laser. After another 2 h incubation cells were washed with PBS and stained with calcein-AM for visualization of live cells and with PI for visualization of dead/late apoptotic cells, according to the manufacture's suggested protocol (Invitrogen). The cells were examined by eliminating the interference of background FL of DOX and ICG with biological inverted microscope (Olympus IX71, JPN).

The cytotoxicity of chemo-photothermal treatment was also evaluated by quantification of apoptotic MCF-7 cells. MCF-7 cells were seeded at a density of 4 $\times$ 10^5 cells/well in 24-well plate and cultured overnight. Cells were treated with/without DINPs containing 6.0 μg/mL DOX and 5.5 μg/mL of ICG for 6 h or combined laser irradiation for 5 min. The cells were harvested, and the Alexa Fluor 488 Annexin V/PI Cell Apoptosis Kit was used to detect and quantify apoptosis by BD Accuri C6 flow cytometer (USA). Annexin V-positive, PI-negative cells were scored as apoptotic. Double-stained cells were considered as necrotic/late apoptotic cells.

For more quantitative evaluation of chemotherapeutic efficacy of DINPs, MCF-7 or MCF-7/ADR cells (1 $\times$ 10^4 cells/well) were seeded into 96-well plate and were incubated in 100 μL of medium with free DOX and DINPs containing the same concentration of DOX. The cells incubated with different concentrations of INPs or free ICG for 2 h were exposed to 1.6 W/cm^2 laser irradiation for different times, and the cells were incubated for another 24 h and quantified to investigate the photothermal therapeutic efficacy. To evaluate the chemo-photothermal treatments of DINPs, we treated MCF-7 or MCF-7/ADR cells with DINPs, DNPs, and INPs. The cells incubated for 2 h were treated

with or without 1.6 W/cm^2 laser for 5 min, and were incubated for another 24 h for MCF-7 cells or another 72 h for MCF-7/ADR cells, and quantified to investigate therapeutic efficacy. The cell viability was quantified by the MTT assay.

Animals and Tumor Model. Female BALB/c nude mice (4−6 weeks old) were purchased from Vital River Laboratory Animal Technology Co. Ltd. (China). Animals received care in accordance with the Guidance Suggestions for the Care and Use of Laboratory Animals. The procedures were approved by Shenzhen Institutes of Advanced Technology, Chinese Academy of Sciences Animal Care and Use Committee. MCF-7 cells (1×10^6) or MCF-7/ADR cells (1×10^7) were administered by subcutaneous injection into the flank region of the mice. Tumor volume was calculated as (tumor length) × (tumor width)^2/2.

Temperature Measurements during Laser Irradiation. PBS (500 μL), free ICG (500 μL, containing 55 μg/mL ICG), INPs (500 μL, containing 55 μg/mL ICG), and DINPs (500 μL, containing 55 μg/mL ICG) was added to centrifuge tubes. The nude mice bearing MCF-7 tumors were intratumoral injected with 150 μL of free ICG, INPs, and DINPs (all containing 55 μg/mL ICG). Mice bearing the MCF-7 tumor were also injected with 150 μL of PBS as control. The tubes and tumors were irradiated by the 808 nm laser at 1 W/cm^2 for 8 min. Region maximum temperatures and infrared thermographic maps were obtained with an infrared thermal imaging camera (Ti27, Fluke, USA).

***In Vivo* Imaging and Biodistribution Analysis.** The nude mice were randomly divided into three groups (three per group). Mice in group 1 as control were intratumoral injected with 150 μL of PBS. Mice in group 2 and group 3 were intratumoral injected with 150 μL of free ICG and DINPs (both containing 55 μg/mL ICG). Images and FL semiquatitative analysis of ICG were taken at 0, 6, 12, and 24 h after injection using the *ex/in vivo* imaging system (CRi maestro, USA) with a 704 nm excitation wavelength and a 735 nm filter to collect the FL signals of ICG. DOX of DINPs was not considered as an optional dye because the EX 480 nm of DOX was not suitable for NIR FL imaging. The mice after injection at 24 h were sacrificed and the organs including heart, liver, spleen, lung, kidneys and tumor were collected for imaging and semiquatitative biodistribution analysis.

***In Vivo* Chemothermal, Photothermal and Chemo-photothermal Treatments.** The mice were divided into groups (six per group) that were intratumoral injected with 150 μL of PBS, free DOX (containing 60 μg/mL DOX), DNPs (containing 60 μg/mL DOX), ICG (containing 55 μg/mL ICG), INPs (containing 55 μg/mL ICG), free ICG and DOX in order (containing 60 μg/mL DOX and 55 μg/mL ICG), DINPs (containing 60 μg/mL DOX and 55 μg/mL ICG), Caelyx (containing 60 μg/mL DOX), and Caelyx plus free ICG (containing 60 μg/mL DOX and 55 μg/mL ICG) . For the laser treatment groups, the tumors of mice were irradiated by the 808 nm laser at 1 W/cm^2 for 5 min. The tumor volumes and changes in body weight of each mouse were recorded. Mice with tumor sizes exceeding 1000 m^3 were euthanatized according to the animal protocol. To further detect the effect of mediated chemo-photothermal therapy *in vivo*, cell apoptosis of tumors at 48 h after treatment was detected by One Step TUNEL apoptosis Assay Kit, and tumors at 12 h and hearts at 17 d after treatment were stained with hematoxylin and eosin.

Statistical Analysis. Data are reported as mean ± SD. The differences among groups were determined using one-way ANOVA analysis followed by Tukey' s post-test; (∗) $P < 0.05$, (∗∗) $P < 0.01$.

Conflict of Interest: The authors declare no competing financial interest.

Acknowledgment. The authors gratefully acknowledge support for this research from the National Natural Science Foundation of China (Grant No. 81071249, 81171446 and 20905050), Guangdong Innovation Team of Low-cost Healthcare, Science and Technology Key Project of Guangdong (2009A030301010) and Shenzhen (CXB201005250029A, JC201005260247A), and the ``Hundred Talents Program'' of Chinese Academy of Sciences.

Supporting Information Available: Additional figures and table as described in the text. This material is available free of charge *via* the Internet at http://pubs.acs.org.

REFERENCES AND NOTES

1. Sun, T. M.; Du, J. Z.; Yao, Y. D.; Mao, C. Q.; Dou, S.; Huang, S. Y.; Zhang, P. Z.; Leong, K. W.; Song, E. W.; Wang, J. Simultaneous Delivery of siRNA and Paclitaxel *via* a "Two-in-One" Micelleplex Promotes Synergistic Tumor Suppression. *ACS Nano* **2011**, *5*, 1483–1494.
2. Mauceri, H. J.; Hanna, N. N.; Beckett, M. A.; Gorski, D. H.; Staba, M. J.; Stellato, K. A.; Bigelow, K.; Heimann, R.; Gately, S.; Dhanabal, M.; *et al*. Combined Effects of Angiostatin and Ionizing Irradiation in Antitumour Therapy. *Nature* **1998**, *394*, 287–291.
3. Lane, D. Designer Combination Therapy for Cancer. *Nat. Biotechnol.* **2006**, *24*, 163–164.
4. Sengupta, S.; Eavarone, D.; Capila, I.; Zhao, G.; Watson, N.; Kiziltepe, T.; Sasisekharan, R. Temporal Targeting of Tumour Cells and Neovasculature with a Nanoscale Delivery System. *Nature* **2005**, *436*, 568–572.
5. Meng, H.; Liong, M.; Xia, T.; Li, Z.; Ji, Z.; Zink, J. I.; Nel, A. E. Engineered Design of Mesoporous Silica Nanoparticles to Deliver Doxorubicin and P-Glycoprotein siRNA to Overcome Drug Resistance in a Cancer Cell Line. *ACS Nano* **2010**, *4*, 4539–4550.
6. Overgaard, J. Combined Adriamycin and Hyperthermia Treatment of a Murine Mammary Carcinoma *in Vivo*. *Cancer Res.* **1976**, *36*, 3077–3081.
7. Johnson, H. A.; Pavelec, M. Thermal Enhancement of Thio-TEPA Cytotoxity. *J. Natl. Cancer Inst.* **1973**, *50*, 903–908.
8. Moon, H. K.; Lee, S. H.; Choi, H. C. *In Vivo* Near-Infrared Mediated Tumor Destruction by Photothermal Effect of Carbon Nanotubes. *ACS Nano* **2009**, *3*, 3707–3713.
9. Sherlock, S. P.; Tabakman, S. M.; Xie, L. M.; Dai, H. J. Photothermally Enhanced Drug Delivery by Ultrasmall Multifunctional FeCo/Graphitic Shell Nanocrystals. *ACS Nano* **2011**, *5*, 1505–1512.
10. Hauck, T. S.; Jennings, T. L.; Yatsenko, T.; Kumaradas, J. C.; Chan, W. C. Enhancing the Toxicity of Cancer Chemotherapeutics with Gold Nanorod Hyperthermia. *Adv. Mater.* **2008**, *20*, 3832–3838.
11. Zhang, L.; Gu, F. X.; Chan, J. M.; Wang, A. Z.; Langer, R. S.; Farokhzad, O. C. Nanoparticles in Medicine: Therapeutic Applications and Developments. *Clin. Pharmacol. & Therapeut.* **2008**, *83*, 761–769.
12. Emerich, D. F.; Thanos, C. G. Targeted Nanoparticle-Based Drug Delivery and Diagnosis. *J. Drug Target.* **2007**, *15*, 163–183.
13. Zheng, M. B.; Gong, P.; Jia, D. X.; Zheng, C. F.; Ma, Y. F.; Cai, L. T. PLGA-Lecithin-PEG Core−Shell Nanoparticles for Cancer Targeted Therapy. *Nano Life* **2012**, *2*, 1250002.
14. Kolishetti, N.; Dhar, S.; Valencia, P. M.; Lin, L. Q.; Karnik, R.; Lippard, S. J.; Langer, R.; Farokhzad, O. C. Engineering of Self-Assembled Nanoparticle Platform for Precisely Controlled Combination Drug Therapy. *Proc. Natl. Acad. Sci. U.S.A.* **2010**, *107*, 17939–17944.
15. Zhang, L.; Chan, J. M.; Gu, F. X.; Rhee, J. W.; Wang, A. Z.; Radovic-Moreno, A. F.; Alexis, F.; Langer, R.; Farokhzad, O. C. Self-Assembled Lipid−Polymer Hybrid Nanoparticles: A Robust Drug Delivery Platform. *ACS Nano* **2008**, *2*, 1696–1702.
16. Wang, A. Z.; Yuet, K.; Zhang, L.; Gu, F. X.; Huynh-Le, M.; Radovic-Moreno, A. F.; Kantoff, P. W.; Bander, N. H.; Langer, R.; Farokhzad, O. C. Chemorad Nanoparticles: A Novel Multifunctional Nanoparticle Platform for Targeted Delivery of Concurrent Chemoradiation. *Nanomedicine* **2010**, *5*, 361–368.
17. Chan, J. M.; Rhee, J. W.; Drum, C. L.; Bronson, R. T.; Golomb, G.; Langer, R.; Farokhzad, O. C. *In Vivo* Prevention of Arterial Restenosis with Paclitaxel-Encapsulated Targeted Lipid-Polymeric Nanoparticles. *Proc. Natl. Acad. Sci. U.S.A.* **2011**, *108*, 19347–19352.
18. Hu, C. M.; Zhang, L.; Aryal, S.; Cheung, C.; Fang, R. H.; Zhang, L. Erythrocyte Membrane-Camouflaged Polymeric Nanoparticles as a Biomimetic Delivery Platform. *Proc. Natl. Acad. Sci. U.S.A.* **2011**, *108*, 10980–10985.
19. Zheng, C. F.; Zheng, M. B.; Gong, P.; Jia, D. X.; Zhang, P. F.; Shi, B. H.; Sheng, Z. H.; Ma, Y. F.; Cai, L. T. Indocyanine

Green-Loaded Biodegradable Tumor Targeting Nanoprobes for *in Vitro* and *in Vivo* Imaging. *Biomaterials* **2012**, *33*, 5603–5609.
20. Manchanda, R.; Fernandez-Fernandez, A.; Nagesetti, A.; McGoron, A. J. Preparation and Characterization of a Polymeric (PLGA) Nanoparticulate Drug Delivery System with Simultaneous Incorporation of Chemotherapeutic and Thermo-optical Agents. *Colloids Surf. B Biointerfaces* **2010**, *1*, 260–267.
21. Gao, Z. G.; Lukyanov, A. N.; Singhal, A.; Torchilin, V. P. Diacyllipid−Polymer Micelles as Nanocarriers for Poorly Soluble Anticancer Drugs. *Nano Lett.* **2002**, *2*, 979–982.
22. Kirchherr, A. K.; Briel, A.; Mäder, K. Stabilization of Indocyanine Green by Encapsulation within Micellar Systems. *Mol. Pharm.* **2009**, *6*, 480–491.
23. Rodriguez, V. B.; Henry, S. M.; Hoffman, A. S.; Stayton, P. S.; Li, X.; Pun, S. H. Encapsulation and Stabilization of Indocyanine Green within Poly(styrene-alt-maleic anhydride) Block-poly(styrene) Micelles for Near-Infrared Imaging. *J. Biomed. Opt.* **2008**, *13*, 014025.
24. Saxena, V.; Sadoqi, M.; Shao, J. Enhanced Photo-stability, Thermal-Stability and Aqueous-Stability of Indocyanine Green in Polymeric Nanoparticulate Systems. *J. Photochem. Photobiol., B* **2004**, *74*, 29–38.
25. Lim, Y. T.; Noh, Y. W.; Han, J. H.; Cai, Q. Y.; Yoon, K. H.; Chung, B. H. Biocompatible Polymer-Nanoparticle-Based Bimodal Imaging Contrast Agents for the Labeling and Tracking of Dendritic Cells. *Small* **2008**, *4*, 1640–1645.
26. Zheng, X. H.; Zhou, F. F.; Wu, B. Y.; Chen, W. R.; Xing, D. Enhanced Tumor Treatment Using Biofunctional Indocyanine Green-Containing Nanostructure by Intratumoral or Intravenous Injection. *Mol. Pharm.* **2012**, *9*, 514–522.
27. Tang, Y.; Lei, T.; Manchanda, R.; Nagesetti, A.; Fernandez-Fernandez, A.; Srinivasan, S.; McGoron, A. J. Simultaneous Delivery of Chemotherapeutic and Thermal-Optical Agents to Cancer Cells by a Polymeric (PLGA) Nanocarrier: an *in Vitro* Study. *Pharm. Res.* **2010**, *27*, 2242–2253.
28. Graff, B. A.; Bjornaes, I.; Rofstad, E. K. Macromolecule Uptake in Human Melanoma Xenografts. Relationships to Blood Supply, Vascular Density, Microvessel Permeability and Extracellular Volume Fraction. *Eur. J. Cancer* **2000**, *36*, 1433–1440.
29. Jain, R. K. Transport of Molecules in The Tumor Interstitium: A Review. *Cancer Res.* **1987**, *47*, 3039–3051.
30. Lamm, D. L. Carcinoma *in Situ*. *Urol. Clinics North Am.* **1992**, *19*, 499–508.
31. Altnoglu, E. I.; Russin, T. J.; Kaiser, J. M.; Barth, B. M.; Eklund, P. C.; Kester, M.; Adair, J. H. Near-Infrared Emitting Fluorophore-Doped Calcium Phosphate Nanoparticles for *in Vivo* Imaging of Human Breast Cancer. *ACS Nano* **2008**, *2*, 2075–2084.
32. Zhang, J.; Jin, W.; Wang, X.; Wang, J.; Zhang, X.; Zhang, Q. A Novel Octreotide Modified Lipid Vesicle Improved the Anticancer Efficacy of Doxorubicin in Somatostatin Receptor 2 Positive Tumor Models. *Mol. Pharm.* **2010**, *7*, 1159–1168.
33. Peng, C. L.; Shih, Y. H.; Lee, P. C.; Hsieh, T. M.; Luo, T. Y.; Shieh, M. J. Multimodal Image-Guided Photothermal Therapy Mediated by ^{188}Re-Labeled Micelles Containing a Cyanine-Type Photosensitizer. *ACS Nano* **2011**, *5*, 5594–5607.
34. Hirsch, L. R.; Stafford, R. J.; Bankson, J. A.; Sershen, S. R.; Rivera, B.; Price, R. E.; Hazle, J. D.; Halas, N. J.; West, J. L. Nanoshell-Mediated Near-Infrared Thermal Therapy of Tumors under Magnetic Resonance Guidance. *Proc. Natl. Acad. Sci. U.S.A.* **2003**, *100*, 13549–13554.
35. Li, W.; Nie, S.; Xie, M.; Chen, Y.; Li, C.; Zhang, H. A Major Green Tea Component, (−)-Epigallocatechin-3-Gallate, Ameliorates Doxorubicin-Mediated Cardiotoxicity in Cardiomyocytes of Neonatal Rats. *J. Agric. Food Chem.* **2010**, *58*, 8977–8982.
36. Fang, R. H.; Aryal, S.; Hu, C. M.; Zhang, L. Quick Synthesis of Lipid-Polymer Hybrid Nanoparticles with Low Polydispersity Using a Single-Step Sonication Method. *Langmuir* **2010**, *26*, 16958–16962.